A co-confined carbonization approach to aligned nitrogen-doped mesoporous carbon nanofibers and its application as an adsorbent

Aibing Chen [a,*,1], Chao Liu [b,1], Yifeng Yu [a], Yongqi Hu [a], Haijun Lv [a], Yue Zhang [a], Shufeng Shen [a], Jian Zhang [c,*]

[a] College of Chemical and Pharmaceutical Engineering, Hebei University of Science and Technology, Shijiazhuang 050018, China
[b] College of Gemmology and Material Technics, Shijiazhuang University of Economic, Huaian Road 136, Shijiazhuang 050031, China
[c] Ningbo Institute of Materials Technology & Engineering, Chinese Academy of Sciences, Ningbo 315201, China

HIGHLIGHTS

- MCNFs were synthesized by a co-confined carbonization method.
- The diameter size of MCNFs with bimodal mesoporous structure can be modulated.
- The obtained MCNFs manifest better adsorption capacity for SO_2, CO_2 and Cd^{2+}.

ARTICLE INFO

Keywords:
Carbon nanofibers
Mesoporous
Nitrogen-doped
Adsorption

ABSTRACT

Nitrogen-doped carbon nanofibers (MCNFs) with an aligned mesoporous structure were synthesized by a co-confined carbonization method using anodic aluminum oxide (AAO) membrane and tetraethylorthosilicate (TEOS) as co-confined templates and ionic liquids as the precursor. The as-synthesized MCNFs with the diameter of 80–120 nm possessed a bulk nitrogen content of 5.3 wt% and bimodal mesoporous structure. The nitrogen atoms were mostly bound to the graphitic network in two forms, *i.e.* pyridinic and pyrrolic nitrogen, providing adsorption sites for acidic gases like SO_2 and CO_2. Cyclic experiments revealed a considerable stability of MCNFs over 20 runs of SO_2 adsorption and 15 runs for CO_2 adsorption. The MCNFs also have a preferable adsorption performance for Cd^{2+}.

1. Introduction

Both one-dimensional (1D) and mesoporous carbon materials are of tremendous interests because of their special structures and promising applications in the fields of electronics, composites, environmental protection, catalysis, etc. [1–4]. Mesoporous carbon nanofibers may combine the advantages of mesoporous structure and the 1D morphology. For example, when MCNFs is used as an adsorbent, 1D mesoporous architecture can provide sufficient porosity as well shortened pathway for the target molecules with the fast adsorption kinetics. Further introducing nitrogen-containing functional groups into the graphitic matrix would benefit MCNFs an improved capacity to capture some acidic gases such as SO_2, SO_3 and CO_2 [5–10]. SO_2 in the atmosphere is apt to threat humans' health and cause acid rain, which has been a serious problem for the ecosystem. Compared with other technologies, the adsorption process by using the solid carbon adsorbent requires simple equipment and does not generate any derived pollutants [11,12]. CO_2, which is the main greenhouse gas to result in global warming, is produced as a flue gas in many industrial processes, and in automobile exhausts [13]. The removal of CO_2 from flue gases by a capture process is necessary prior to their release to the atmosphere. Recently, nitrogen-functionalized mesoporous silica and carbon materials have been extensively used as a sorbent for CO_2 capture due to the strong chemical interaction between CO_2 molecules and sorbents and they show relatively good performance resulting from the combination of their high surface area and the basicity of nitrogen-containing groups [14,15].

Electrospinning technique is usually applied to produce porous MCNFs by the addition of porogens or subsequent activation processes [16,17], but its industrialization is still limited by the difficulties in controlling synthesis parameters and enhancing the

* Corresponding author. Tel.: +86 311 8863 2043.
E-mail addresses: chen_ab@163.com (A. Chen), jzhang@nimte.ac.cn (J. Zhang).
[1] These authors contributed equally to this work.

productivity. There are many studies on the templating approach to MCNFs [5,6,18–20]. For instance, MCNFs were prepared by carbonizing the proper precursors within suitable templates having long tunnels, such as anodic aluminum oxide (AAO) membrane and crab shell. This method allows adjusting the structural properties of MCNFs such as pore size and surface functionality. Nevertheless, the evaporation induced self-assembly process comprises multiple steps and is thus time-consuming. Few reports showed that the MCNFs can be directly synthesized via carbonizing 1D polymer while the obtained MCNFs displayed a low surface area and infinite pore volume [21,22].

Ionic liquids (ILs) have negligible vapor pressure, wide liquid range, high thermal stability and capacity to be incorporated into porous templates avoiding high pressure and evaporation. Most recently, the advantages of ILs as a new carbon source have attracted many interests for the synthesis of carbon materials. Imidazolium- and pyridinium-based ILs containing dicyanamide anions have been employed to produce nitrogen-doped carbons materials with favorable structures [23–25]. In these studies, all the ILs contain cross-linkable functional groups (so called task-specific ionic liquids, TSILs) such as nitrile, as the intermediate polymeric structures during thermal decomposition, whereas the synthesis of TSILs is complex and costly. Herein we present a simple co-confined carbonization method, using a cheap ILs (1-dodecyl-3-methylimidazolium bromide, C_{12}MIMBr) as the precursor, to prepare nitrogen-doped MCNFs. Both the AAO membrane and tetraethylorthosilicate (TEOS) were used as the co-confined templates. The arrayed MCNFs possessed uniformed morphology and typical mesoporous characteristic, contained 5.3 wt% of nitrogen in bulk, and displayed a preferable performance for the adsorption of SO_2, CO_2 and Cd^{2+}.

2. Experimental

2.1. Synthesis of AAO template

The AAO membrane was synthesized by the method reported in previous work with some modification [26]. For a typical synthesis, the AAO membrane with an average pore diameter of 80 nm were prepared by anodizing aluminum foil (purity 99.999%) at 40 V in 0.3 M oxalic acid solution for 12 h, followed by removing the membrane with a mixed acid of 6% phosphoric acid and 4% chromic acid (v:v = 1:1), then for the second anodizing with the same condition for 10 h. The specimen was then dipped into saturated cupric chloride to etching the unreacted aluminum, followed by adjusting the pore diameter in a 5 wt% phosphoric acid solution at 25 °C for 40 min. The AAO templates with different pore diameters were obtained through changing the anodizing voltage.

2.2. Synthesis of MCNFs

1.0 g of C_{12}MIMBr (Shanghai Cheng Jie Chemical Co., Ltd.) was dissolved in 3 mL of ethanol and stirred for 30 min. AAO membranes were added into the solution in vacuum for 40 min and dried at 60 °C. In order to make the AAO membranes fully infiltrated with ionic liquid, the above step repeated for several times. The carbonization was conducted in N_2 at 600 °C for 2 h with a heating rate of 1 °C min^{-1}, after which the AAO templates were removed by using 10% aqueous HF. The products were referred as MCNF-*x*, where *x* indicates the diameters of the MCNFs. For the co-confined synthesis, typically, 1.0 g of C_{12}MIMBr was dissolved in 3.0 mL of ethanol followed by adding 0.5 g TEOS and 1.0 mL formic acid, and then stirred for 30 min. The following procedure was identical to that of MCNF-*x*. The obtained samples were denoted as MCNF-*x* – *y*, where *y* indicates the mass ratio of TEOS: ILs.

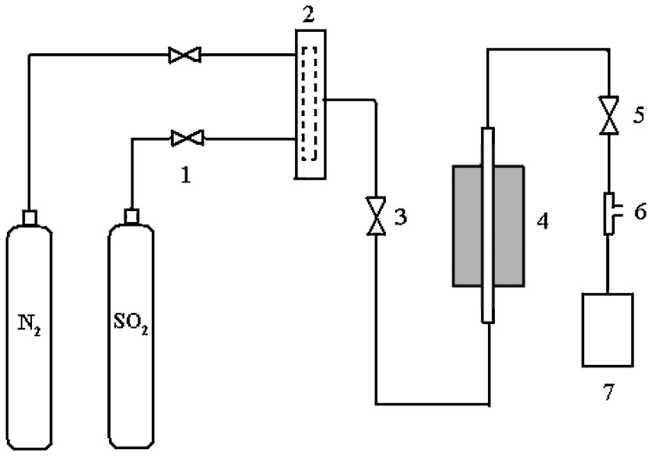

Fig. 1. Schematic diagram of the experimental setup for SO_2 adsorption. 1, 3, 5, mass flow rate controller; 2, gas mixing chamber; 4, fixed-bed reactor; 6, SO_2 adsorber; 7, gas analyzer.

2.3. Characterization

X-ray diffraction pattern (XRD) were obtained on a Rigaku D/MAX-2500 X-ray diffraction system(Cu Kα radiation, λ = 1.5406 Å) operated at 40 kV and 40 mA. Scanning electron microscopy (SEM) and transmission electron micrographs (TEM) images were taken on a Hitachi S4800 microscope working at 20.0 kV and a JEOL JEM-2010 electron microscope, respectively. Nitrogen adsorption–desorption isotherms were evaluated on a Micrometitics TriStar 3020 volumetric adsorption analyzer at −196 °C. The Brunauer–Emmett–Teller (BET) method was utilized to calculate the specific surface area of each sample while the average pore size distribution was derived from the desorption branch using the Barrett–Joyner–Halenda (BJH) method. The total pore volume was estimated from the N_2 amount adsorbed at a relative pressure of $P/P_0 = 0.97$. Raman measurements were performed under ambient conditions using a 532 nm (2.33 eV) laser in the back-scattering configuration on a Jobin-Yvon HR800 Spectrometer. X-ray Photoelectron Spectroscopy (XPS) spectra were obtained using an Axis Ultra spectrometer (Kratos, UK). A mono Al-Kα (1486.6 eV) X-ray source was used at a power of 225 W (15 kV, 15 mA). To correct the surface charge effect, binding energies were calibrated using the C1s hydrocarbon peak at 284.8 eV. Element analysis was achieved using an Elementar Vario Micro Cube. Thermogravimetric (TG) analysis was achieved using Q 600 of TA Instruments-Waters 5 °C min^{-1} under air atmosphere.

2.4. Adsorption

The experimental apparatus is schematically shown in Fig. 1. 0.1 g MCNFs was put in the sorption bed and the gas flow rate was controlled by mass flow controllers. The adsorbing experiment was carried out using a mixed gas composed of N_2, O_2 (5%, v/v) and SO_2 (2400 ppmv) at 20 °C. The mixed gas flows through the sorption bed of length 350 mm with inner diameter 6 mm at a rate of 8 dm^3 min^{-1}. The SO_2 content in the effluent was analyzed by a hand-held combustion analyzer (Model KM940, Kane International Limited). The sorption bed was considered saturated with SO_2 when the concentration of SO_2 in effluent was the same as that in the input stream. The breakthrough capacity of the sorbent (*Q*, mg g^{-1}) was calculated using the followed formula:

$$Q = \int (C_0 - C) \cdot v \cdot M/(m \cdot V_m)\, dt$$

M is the molar weight of SO_2, g mol^{-1}; C_0 is the concentration of SO_2 in input stream and C is the detected concentration of SO_2 in the effluent gas, ppmv; v is the flow rate of the mixed gas, dm^3 min^{-1}; V_m is the molar volume of SO_2, dm^3 mol^{-1}; m is the mass of adsorbent filled in the sorption bed, g; t is the adsorb balance time of SO_2, min. CO_2 adsorption isotherms were evaluated on a Micrometitics TriStar 3020 volumetric adsorption analyzer and the samples was regenerated at 180 °C for 4 h in air.

The adsorption experiment of Cd^{2+} was carried out as follows: 50 mg of the samples were added into 15 mL solution of $Cd(NO_3)_2$ (0.5 M), at 25 °C with continued stirring for 12 h. After filtration and separation, the samples were washed with distilled water till no Cd^{2+} can be detection. Then the samples were dried at 100 °C followed by TG tested to (in air) to measure the absorbed ions content in the samples.

3. Results and discussion

The whole process of the synthesis can be schematically described in Scheme 1. A homogeneous solution containing C_{12}MIMBr and ethanol as solvent, with or without the presence of TEOS, is infiltrated into the nano-channels of AAO membrane in vacuum. For the case without TEOS, the acidic surface of AAO adsorbs Br^- firstly and subsequently $[C_{12}MIM]^+$ ions [27]. The ILs fragments are adsorbed on the interior surface of AAO by the electrostatic force. With the evaporation of ethanol solvent, more and more ILs staying at the outer surface of channels are adsorbed inside the channels of AAO under the capillary force. The material is then carbonized in a flow of ultrapure N_2 while the ILs starts to decompose and transform into particular carbon inside the channels of AAO. To confine the shrinkage during carbonization, TEOS is added as a second confined template. TEOS and ILs can be mixed to form a uniform solution. After the carbonizing of ILs and the removing of templates, the ordered MCNFs containing many uniform mesopores are obtained. In fact, experiment results manifest that ordered MCNFs with uniform mesopore cannot be obtained through direct carbonizing the conventional ILs without the adding of AAO or TEOS. Therefore, we propose a "co-confined carbonization method" for the MCNFs synthesis, in which the co-confined effect is brought by the addition of both AAO and TEOS. This concept can be universal by using other types of ILs as precursor to produce MCNFs (Fig. S1).

Supplementary Fig. S1 related to this article can be found, in the online version, at http://dx.doi.org/10.1016/j.jhazmat.2014.05.045.

3.1. Characterization of the materials

Fig. 2 shows the SEM images of MCNF-80, MCNF-100, MCNF-120, MCNF-80-0.25, MCNF-80-0.5 and MCNF-80-1.0. With the absence of TEOS, the produced material displayed the fibrous morphology benefiting from the spatial confinement effect of the AAO template (Fig. 2a). However, the surface of fibers was quite rough and some fractured pieces can be observed, due to the weak interaction between the ILs and the inner wall of channels that induced the severe decomposition and shrinkage of ILs during carbonization. The time of impregnation process can slightly affect the morphology of produced fibers. When impregnation step was repeated, the fibers became longer and displayed quite uniformly. The average diameter of MCNFs was found to increase with the channel size of AAO and it ranged from 80 to 120 nm, as shown in Fig. 2a–c. TEM image of MCNF-80 sample in Fig. 2a revealed that the fibers were constructed by small carbon particles, in accordance with the SEM results.

When TEOS was introduced as the co-confined template with an appropriate amount, the as-synthesized MCNFs became more uniform with an almost smooth surface being free of individual particles (Fig. 2d). It can be regarded that at the elevated temperature, ILs were carbonized in the confined space formed by TEOS-derived silica nanoparticles and AAO. After the AAO and silica templates were removed by etching, MCNFs with interconnected pores can be produced. Meanwhile, the TEOS with a strong interaction with ILs and AAO channel can prevent the MCNFs contract during carbonization (Scheme 1). As a consequence, the quality of MCNFs was significantly improved even under the same carbonization condition. We note that both confined space and strong interaction with the templates were necessary for the synthesis of MCNFs by using the conventional ILs. However, as we continuously increased the mass ratio of TEOS to ILs to 1.0, the fibrous structure was destroyed and many cracked pieces appeared due to the steric hindrance effect of the excessive silica particles (Fig. 2f).

Table 1
Textural properties of MCNF-80, MCNF-80-0.25 and MCNF-80-0.5.

Sample	S_{BET} (m^2 g^{-1})	V_{BJH} (cm^3 g^{-1})	Average pore size (nm)
MCNF-80	116.3	0.09	3.8/7.6
MCNF-80-0.25	183.2	0.19	3.8/7.0
MCNF-80-0.5	256.8	0.36	3.8/5.6

The effect of TEOS/ILs ratio on the structure of MCNFs was detailed by TEM and XRD characterizations. Typical images of MCNF-80, MCNF-80-0.25 and MCNF-80-0.5 were illustrated in Fig. 3a–c. Different from MCNF-80 with the irregular walls, MCNF-80-0.25 and MCNF-80-0.5 displayed the relatively complete feature of nanofibers, in agreement with the SEM results in Fig. 2. Both high-resolution TEM image and XRD pattern in Fig. 3d–e reported a partially graphitic structure of MCNF-80-0.5. The lattice spacing distance was estimated to be around 0.36 nm being larger than that of pure graphite crystal, which is usually explained by the doping of nitrogen atoms in the graphitic matrix [28]. Three reflections at $2\theta = 25.8$, 43, 53 and 79° can be identified in the XRD pattern in Fig. 3e and corresponded to the (0 0 2), (1 0 0), (0 0 4) and (1 1 0) planes of graphite, respectively. The d_{002} value was calculated to be 0.36 nm, being close to the TEM result, according to the Bragg formula.

N_2 adsorption–desorption isotherms and pore size distribution of MCNFs are depicted in Fig. 4. It can be observed that all isotherm curves of the MCNFs samples exhibited a hysteresis loop in a wide P/P_0 range of 0.4–1.0, demonstrating the mesoporous characteristic of the materials. This can be considered as accumulated pores of carbon particles and the space among the MCNFs after etching of the AAO and TEOS templates. The curves in Fig. 4a can be classified as type IV isotherm with a pronounced H3-type hysteresis loop, corresponding to a slit-shaped mesopore. Two kinds of mesopores centered at 3.8 and 5.6–7.6 nm were observed in Fig. 4b. As compared with MCNF-80, MCNF-80-0.25 and MCNF-80-0.5 possessed more mesopores centering at about 3.8 nm. Considering the peak position is identical, we attributed it to the spontaneously formed porosity inside the derived carbon particles via the decomposition of ILs aggregates being independent with the participation of TEOS. With the increasing amount of TEOS, the summit of bigger mesopore at about 7.6 nm shifted downwards to 7.0 and further 5.6 nm. We therefore attributed the mesopores at around 5.6 nm to the accumulating of the carbon particles and the removal of silica nanoparticles. MCNF-80 shrunk irregularly due to the weak interface force between ILs and AAO walls during carbonization. With the TEOS as the co-confined template, the structure of the nanofibers was strengthened and the shrinkage was greatly restricted to result in a complete morphology of fibrous carbon. The TEOS-derived silica nanoparticles also benefited a significant increase of the pore volume (Table 1).

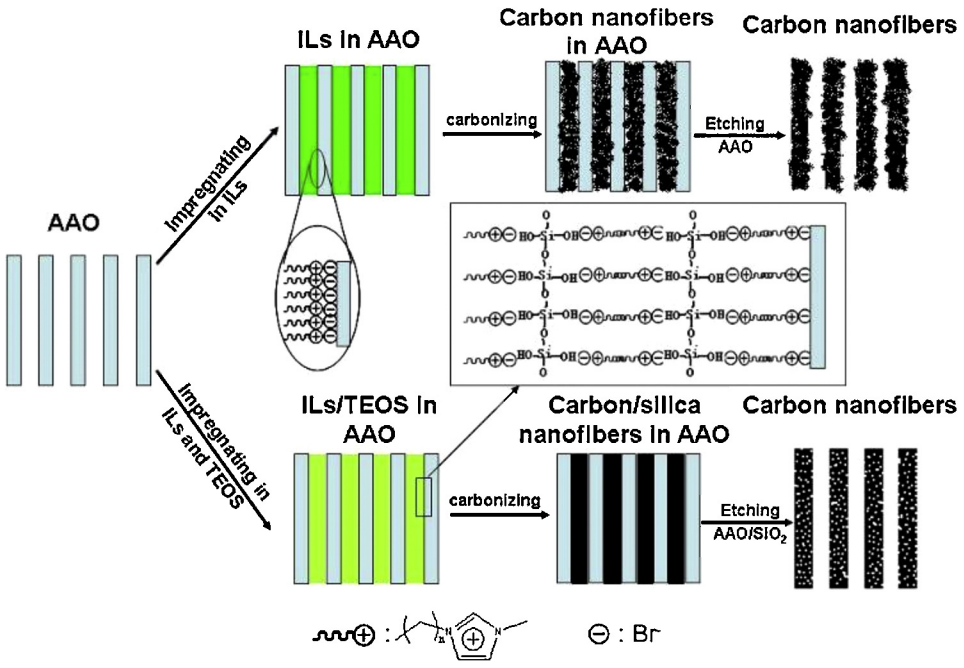

Scheme 1. Synthesis procedure of MCNFs through AAO and TEOS confined carbonization.

The elemental analysis showed that the overall nitrogen content of MCNF-80-0.5 was 5.3 wt% in bulk. In order to clarify the chemical states of nitrogen dopant, we examined the C*1s* and N*1s* XPS spectra of the MCNF-80-0.5 sample (Fig. 5). Three elementary components were identified in the C*1s* spectrum (Fig. 5a). The main peak at 284.8 eV corresponded to the graphite-like sp^2 C, indicating that most of the C atoms were arranged in a conjugated honeycomb lattice. Two small peaks at 286.0 and 289.2 eV reflected different bonding structure of the C—N bonds and were assigned to the N-sp^2 C and N-sp^3 C bonds, respectively, which may originate from the substitution of N atoms to the defects or the edge of the graphitic layer [29]. Deconvolution of the N*1s* spectrum (Fig. 5b) reported two components, i.e. pyrrolic and/or pyridonic nitrogen (400.6 eV), and pyridinic nitrogen (398.7 eV) [30].

The Raman spectrum of MCNF-80-0.5 is displayed in Fig. 6. Two obvious peaks at ~1340 and ~1586 cm^{-1} can be related with the *D* and *G* bands, respectively. The *D* band, commonly centering between 1200 and 1450 cm^{-1} and indicating a reduction in the symmetry of the graphitic lattice, was caused by atomic substitution or structural defects [31]. The *G* band was attributed to the E2g vibration mode that is present due to the sp^2 bonded graphitic carbons [30]. The intercalation of nitrogen atoms resulted in a slightly downward shift of *G* band [30].

3.2. Adsorption tests

As seen in Fig. 7a, in a diluted flow of SO_2 (2400 ppmv), the breakthrough time increased remarkably from MCNF-80 to MCNF-80-0.5. Longer breakthrough time revealed an enhanced adsorption capacity and faster response to the acidic pollutant. MCNF-80-0.5 possessed a satisfactory adsorption capacity of 40.2 mg g^{-1}, being 2.9 times that of MCNF-80. It is worth noting that the SO_2

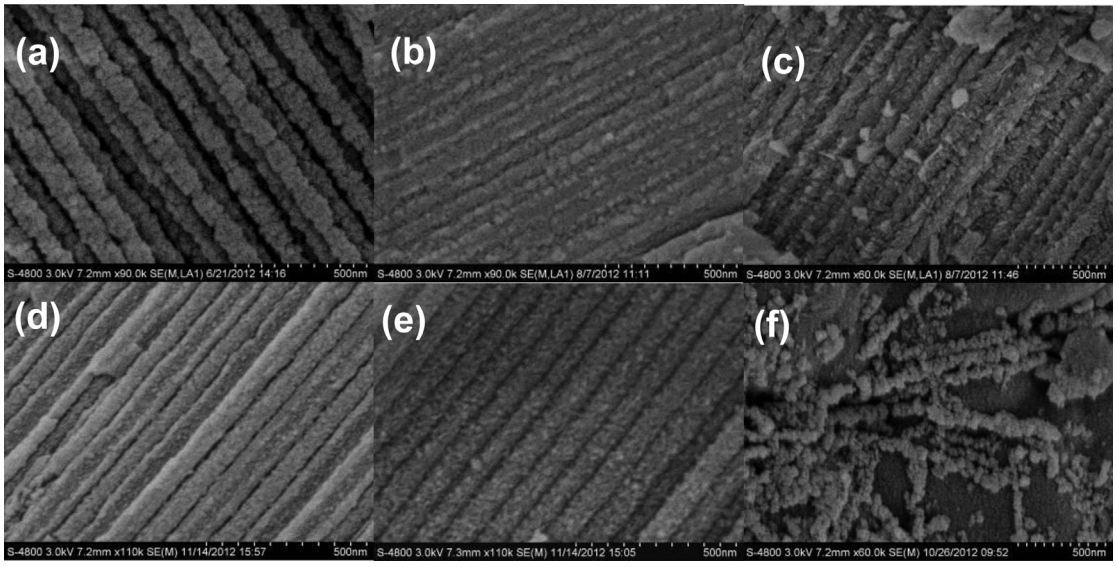

Fig. 2. SEM images of the produced carbon nanofibers: (a) MCNF-80, (b) MCNF-100, (c) MCNF-120, (d) MCNF-80-0.25, (e) MCNF-80-0.5, and (f) MCNF-80-1.0.

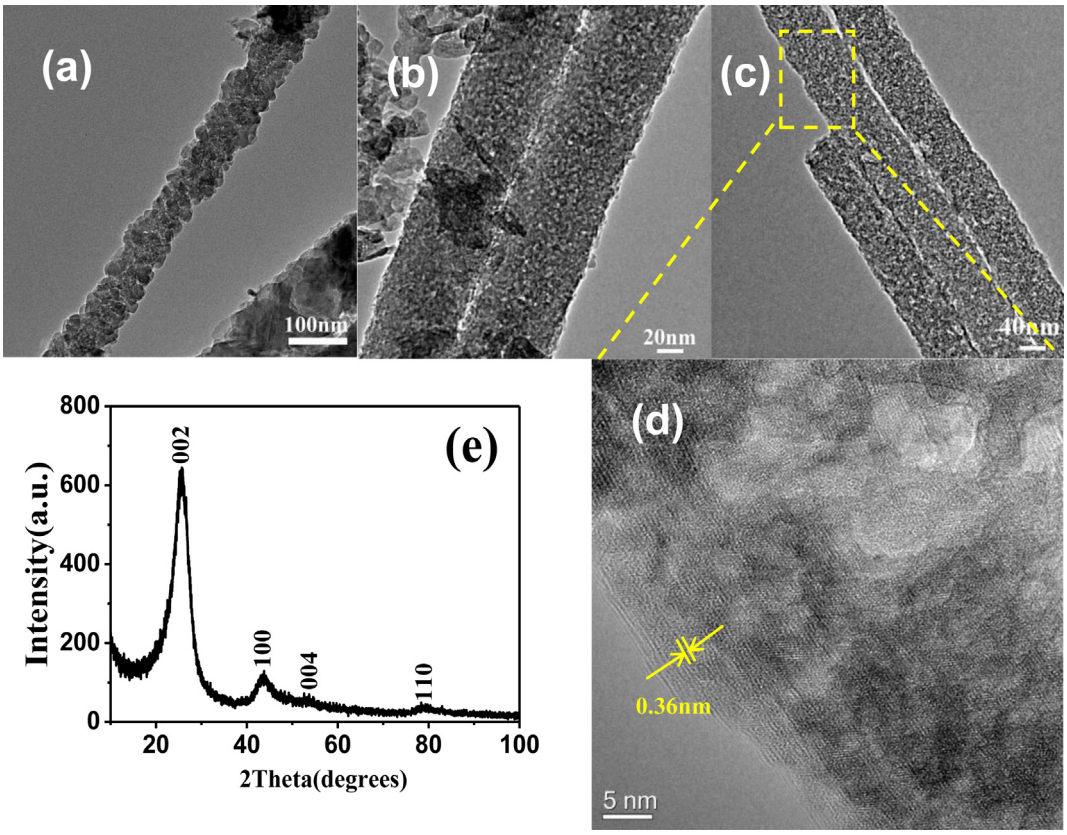

Fig. 3. TEM images of MCNF-80 (a), MCNF-80-0.25 (b), MCNF-80-0.5 (c), HRTEM of MCNF-80-0.5 edge (d) and X-ray diffraction of MCNF-80-0.5 (e).

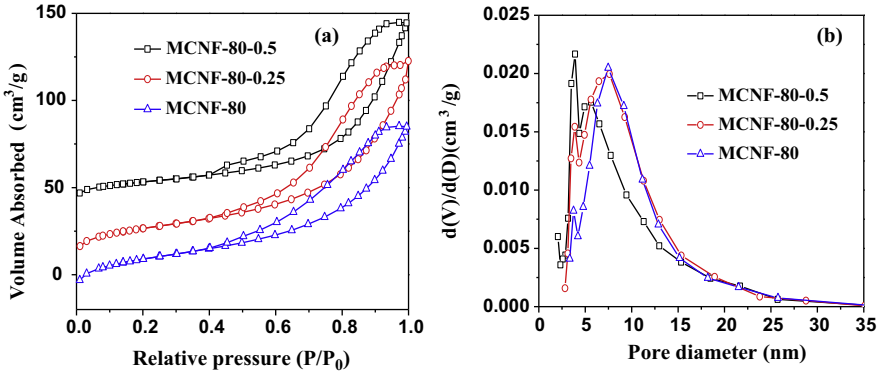

Fig. 4. Nitrogen adsorption–desorption isotherms (a) and pore size distributions (b) of MCNFs.

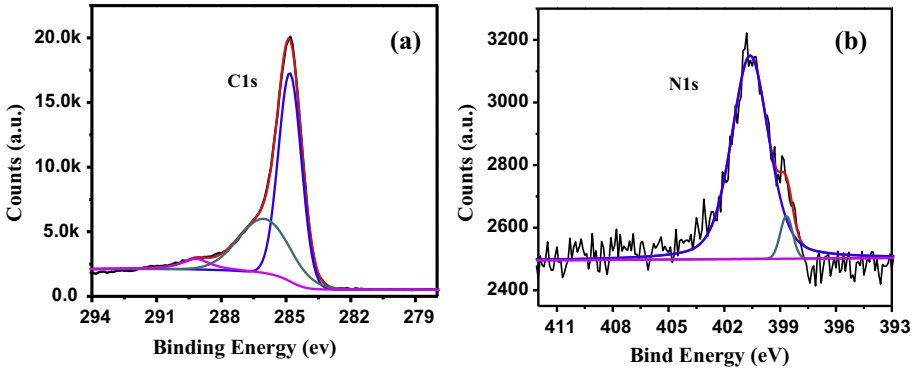

Fig. 5. XPS spectrum of MCNF-80-0.5: C*1s* spectrum (a) and N*1s* spectrum (b).

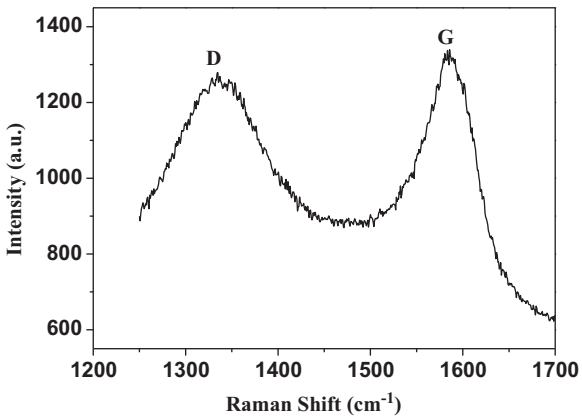

Fig. 6. Raman spectrum of MCNF-80-0.5.

adsorption capacity even approach that of the reported activated carbon fibers (ACFs) [32], while the surface area of the MCNFs is much lower than that of ACFs (ca. 1500 $m^2 g^{-1}$). The XPS result in Fig. 5 showed that the main chemical states of nitrogen in MCNFs were pyrrolic and/or pyridonic nitrogen. The SO_2 molecules might be physically adsorbed on MCNFs through hydrogen bond with pyrrolic-N or neighboring hydroxy pyridonic-N, and the nitrogen-contain species (Fig. 7c). It is also plausible that surface oxygen functional groups like hydroxyls tend to chemically bind SO_2 to produce sulfite ions and the derived sulfate ions after the contact with O_2 [33], which unfortunately contributes to the irreversible capacity of MCNFs. The cyclic adsorption tests of SO_2 showed that the adsorption capacity of MCNFs gradually decreased for about 7% during the first six cycles but remained almost unchanged in the following 14 cycles (Fig. 7d).

To comprehend the details the adsorption process, we employed the XPS technique to check the difference of surface chemical state of fresh and used MCNF-80-0.5 samples. Fig. 8 presents the S*2p* and N*1s* spectra of SO_2-saturated MCNF-80-0.5 after desorption at 120 °C for 2 h. The sample showed two individual peaks at 168.4 and 163.9 eV, respectively, which represent SO_3^{2-}/SO_4^{2-} and S^{2-} according to the peak standard card. The SO_3^{2-}/SO_4^{2-} derived from the catalysis reaction of SO_2 on the surface of N-doped MCNFs [32,34]. The S^{2-} perhaps derived from the production of disproportionation reaction of SO_2. The N*1s* peak positions (centered at 400.6 and 398.7 eV) have no obvious change compared to that of before adsorption of SO_2 (Fig. 5). So it can be speculated that the favorable SO_2 cyclic adsorption capacity can be remained mainly due to the weak physical adsorption on the alkaline caused by the N species.

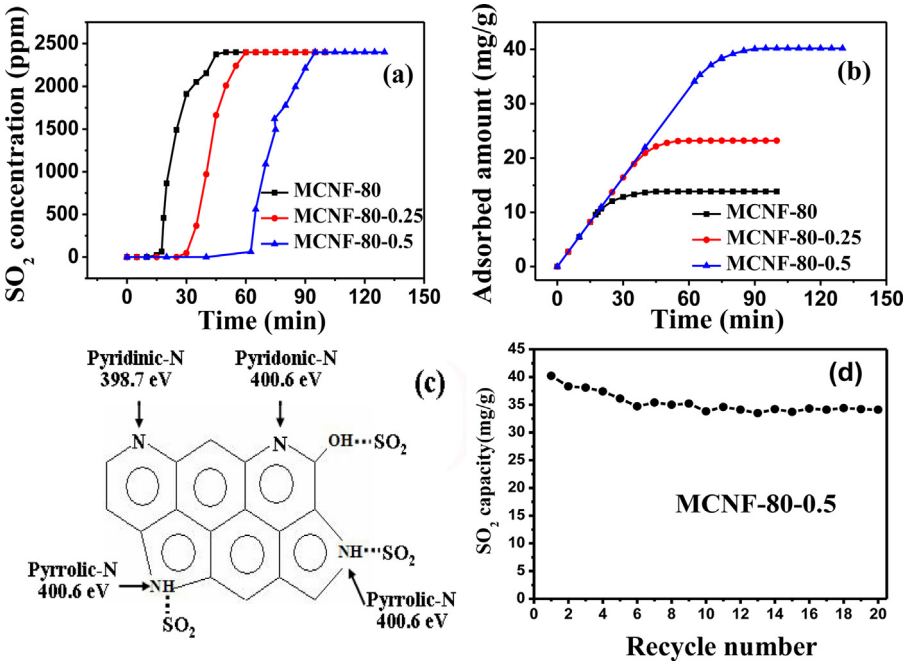

Fig. 7. Breakthrough curves for SO_2 passing the MCNFs bed (a); breakthrough capacity (b); absorption schematic diagram for SO_2 (c) and regeneration cycles (d).

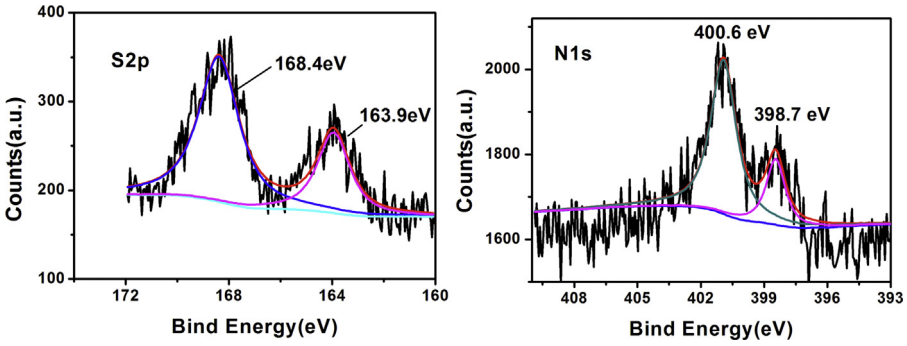

Fig. 8. XPS S*2p* region for MCNF-80-0.5: adsorpted SO_2 (a) and desorpted at 120 °C for 2 h (b).

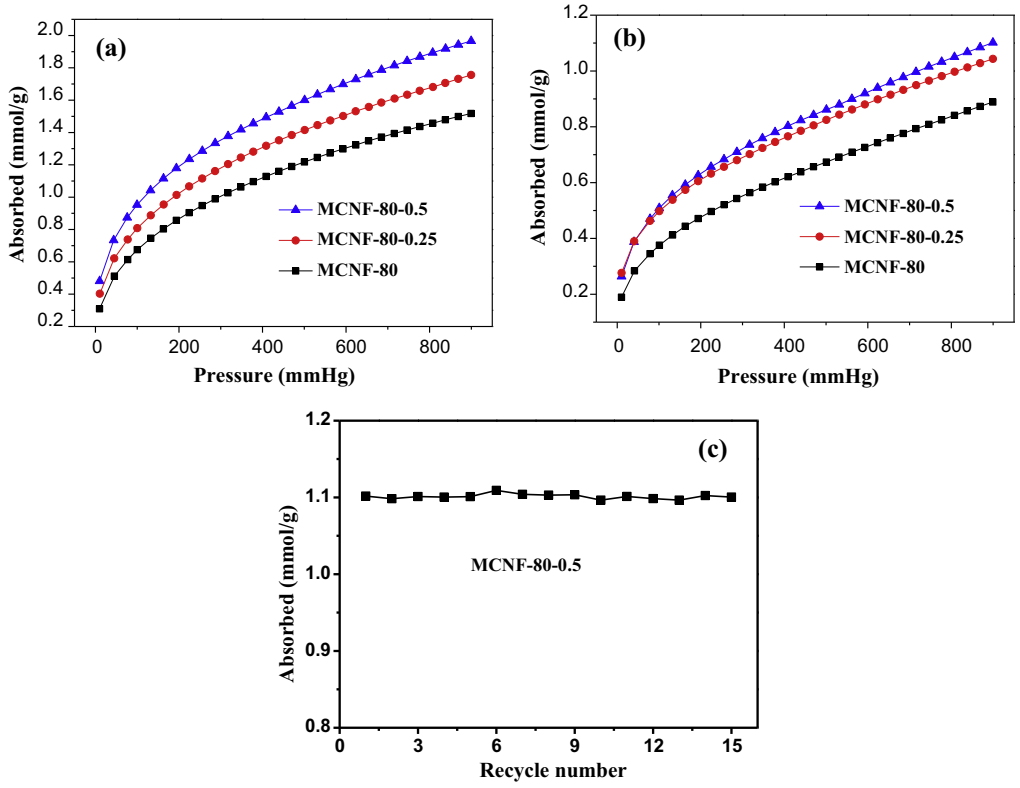

Fig. 9. CO_2 adsorption isotherms at 25 (a), 80 °C (b) of the MCNFs and the regeneration cycles of MCNF-80-0.5 at 80 °C (c).

Porous carbons and their counterparts doped with nitrogen are attracting wide interest for CO_2 adsorption due to their high surface areas and the enhanced interactions by the presence of nitrogen-containing functionalities [35,36]. Herein, CO_2 adsorption isotherms of the MCNFs samples were shown in Fig. 9. At 25 °C and 900 mmHg, the adsorption capacity of all the samples were much higher than the reported KOH-activated graphite nanofibers (1.3 mmol g^{-1}) [37]. The adsorption capacity of MCNF-80-0.5 (2.0 mmol g^{-1}) is higher than that the other MCNFs samples or hard-templated mesoporous carbon (1.51 mmol g^{-1}) (Fig. 9a) [38]. While the temperature of flue gas containing CO_2 after desulfurization is about 60–80 °C, therefore the capture of CO_2 at the relatively high temperature has more significant. So the high temperature adsorption was tested (Fig. 9b). The adsorption capacities of the samples deteriorate with increasing temperature. The adsorption capacity of MCNF-80-0.5 only decreased 0.8 mmol g^{-1} at 80 °C. However, the adsorption capacity of other carbon materials, such as mesoporous CN spheres, reduced move obviously (from 2.90 to 0.97 mmol g^{-1}, at 75 °C) [39]. For CO_2 adsorption, physical adsorption is the main adsorption form to pure carbon, while the chemical adsorption is the main adsorption form to the MCNFs, which is attributed to the presence of nitrogen-containing functionalities that can promote CO_2 capture. With the adsorption temperature increasing, the physical adsorption decreased more obviously than the chemical adsorption. Therefore the MCNFs manifested better adsorption capacity at high temperature. The cyclic adsorption tests of CO_2 at 80 °C showed that the adsorption capacity of MCNF-80-0.5 at equilibrium has no obvious decreasing even after 15 cycles (Fig. 9c).

What is more, one promising application of the nitrogen-doped carbon is to adsorb heavy metal ions like Cd^{2+} from the polluted water. The adsorption capacities of Cd^{2+} of MCNFs were also measured based on TG curves. As shown in Fig. 10, all the MCNFs samples have much higher adsorption capacities for

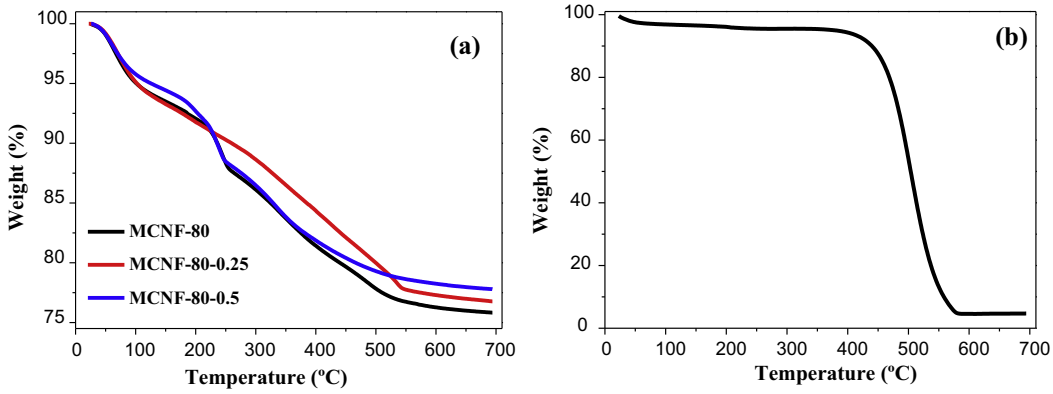

Fig. 10. TG curves of MCNFs (a) and FDU-15 (b) after absorption of Cd^{2+} for 12 h in an air flow.

Cd^{2+} than mesoporous carbon FDU-15 with a BET surface area of 879 $m^2\,g^{-1}$ and pore volume of 1.08 $cm^3\,g^{-1}$. The capacities were 27.4, 25.0 and 24.5 mmol g^{-1} for MCNF-80-0.5, MCNF-80-0.25 and MCNF-80, respectively. However, the capacity of FDU-15 was only 0.39 mmol g^{-1}. The improved capacity also can be attributed to the nitrogen-containing functionalities and the special pore structures of the MCNFs.

4. Conclusions

Nitrogen-doped MCNFs have been prepared by using template method, with conventional ILs as precursors and AAO as template. The pore structure and surface area of MCNFs have a remarkable improvement by introducing TEOS as the co-confined template. The diameter size of MCNFs can be modulated by changing the pore diameter of the templates. A possible formation mechanism is proposed to interpret the synthetic process of MCNFs. The obtained MCNFs manifest better adsorption capacity for SO_2, CO_2 and Cd^{2+}.

Acknowledgements

The work was supported by the projects granted by the Natural Science Foundation of China (20906019) and Science and Technology Research Projects in Hebei Universities (QN20131069 and ZD20131032).

References

[1] Q. Cao, J.A. Rogers, Ultrathin films of single-walled carbon nanotubes for electronics and sensors: a review of fundamental and applied aspects, Adv. Mater. 21 (2009) 29–53.
[2] S.R. Bakshi, D. Lahiri, A. Agarwal, Carbon nanotube reinforced metal matrix composites – a review, Int. Mater. Rev. 55 (2010) 41–64.
[3] X. Pan, X. Bao, The effects of confinement inside carbon nanotubes on catalysis, Acc. Chem. Res. 44 (2011) 553–562.
[4] J. Ji, X. Duan, G. Qian, X. Zhou, D. Chen, W. Yuan, In situ production of Ni catalysts at the tips of carbon nanofibers and application in catalytic ammonia decomposition, Ind. Eng. Chem. Res. 52 (2013) 1854–1858.
[5] C.L. Mangum, K.R. Benak, J. Economy, K.L. Foster, Surface chemistry, pore sizes and adsorption properties of activated carbon fibers and precursors treated with ammonia, Carbon 39 (2001) 1809–1820.
[6] P. Davini, Flue gas desulphurization by activated carbon fibers obtained from polyacrylonitrile by-product, Carbon 41 (2003) 277–284.
[7] M. Seredych, T.J. Bandosz, Role of microporosity and nitrogen functionality on the surface of activated carbon in the process of desulfurization of digester gas, J. Phys. Chem. C 112 (2008) 4704–4711.
[8] Y.C. Yu, X. Fan, L. Yu, T.J. Bandosz, Z. Zhao, J. Qiu, Adsorptive removal of thiophenic compounds from oils by activated carbon modified with concentrated nitric acid, Energy Fuels 27 (2013) 1499–1505.
[9] T.J. Bandosz, M. Seredych, J. Allen, J. Wood, E. Rosenberg, Silica-polyamine-based carbon composite adsorbents as media for effective hydrogen sulfide adsorption/oxidation, Chem. Mater. 19 (2007) 2500–2511.
[10] M. Seredych, T.J. Bandosz, Desulfurization of digester gas on wood-based activated carbons modified with nitrogen: importance of surface chemistry, Energy Fuels 22 (2008) 850–859.
[11] S. Sumathi, S. Bhatia, K.T. Lee, A.R. Mohamed, Selection of best impregnated palm shell activated carbon (PSAC) for simultaneous removal of SO_2 and NO_x, J. Hazard. Mater. 176 (2010) 1093–1096.
[12] J. Xiang, Q.S. Zhao, S. Hu, L.S. Sun, S. Su, P. Fu, A. Zhang, R. Qiu, H. Chen, M. Xu, Experimental research and characteristics analysis of alumina-supported copper oxide sorbent for flue gas desulfurization, Asia-Pac. J. Chem. Eng. 2 (2007) 182–189.
[13] J.A. Thote, K.S. Iyer, R. Chatti, N.K. Labhsetwar, R.B. Biniwale, S.S. Rayalu, In situ nitrogen enriched carbon for carbon dioxide capture, Carbon 48 (2010) 396–402.
[14] Z. Liang, B. Fadhel, C.J. Schneider, A.L. Chaffee, Adsorption of CO_2 on mesocellular siliceous foam iteratively functionalized with dendrimers, Adsorption 15 (2009) 429–437.
[15] T. Seki, Y. Kokubo, S. Ichikawa, T. Suzuki, Y. Kayaki, T. Ikariya, Mesoporous silica-catalysed continuous chemical fixation of CO_2 with N,N,-dimethylethylenediamine in supercritical CO_2: The efficient synthesis of 1,3-dimethyl-2-imidazolidinone, Chem. Commun. 45 (2009) 349–351.
[16] C. Kim, B.T.N. Ngoc, K.S. Yang, M. Kojima, Y.A. Kim, Y.J. Kim, M. Endo, S.C. Yang, Self-sustained thin webs consisting of porous carbon nanofibers for super capacitors *via* the electrospinning of polyacrylonitrile solutions containing zinc chloride, Adv. Mater. 19 (2007) 2341–2346.
[17] E.J. Ra, T.H. Kim, W.J. Yu, K.H. An, Y.H. Lee, Ultramicropore formation in PAN/camphor-based carbon nanofiber paper, Chem. Commun. 46 (2010) 1320–1322.
[18] B. Fang, M. Kim, S.Q. Fang, J.H. Kim, D.P. Wilkinson, J. Ko, J.S. Yu, Facile synthesis of open mesoporous carbon nanofibers with tailored nanostructure as a highly efficient counter electrode in CdSe quantum-dot-sensitized solar cells, J. Mater. Chem. 21 (2011) 8742–8748.
[19] Y. Gogotsi, R.K. Dash, G. Yushin, T. Yildirim, G. Laudisio, J.E. Fischer, Tailoring of nanoscale porosity in carbide-derived carbons for hydrogen storage, J. Am. Chem. Soc. 127 (2005) 16006–16007.
[20] G. Cui, L. Zhi, A. Thomas, U. Kolb, I. Lieberwirth, K. Müllen, One-dimensional porous carbon/platinum composites for nanoscale electrodes, Angew. Chem. Int. Ed. 119 (2007) 3534–3537.
[21] X. Feng, Y. Liang, L. Zhi, A. Thomas, D. Wu, I. Lieberwirth, U. Kolb, K. Müllen, Synthesis of microporous carbon nanofibers and nanotubes from conjugated polymer network and evaluation in electrochemical capacitor, Adv. Funct. Mater. 19 (2009) 2125–2129.
[22] C. Li, X. Yin, L. Chen, Q. Li, T. Wang, Porous carbon nanofibers derived from conducting polymer: synthesis and application in lithium-ion batteries with high-rate capability, J. Phys. Chem. C 113 (2009) 13438–13442.
[23] X. Wang, S. Dai, Ionic liquids as versatile precursors for functionalized porous carbon and carbon–oxide composite materials by confined carbonization, Angew. Chem. Int. Ed. 49 (2010) 6664–6668.
[24] T.P. Fellinger, F. Hasché, P. Strasser, M. Antonietti, Mesoporous nitrogen-doped carbon for the electrocatalytic synthesis of hydrogen peroxide, J. Am. Chem. Soc. 134 (2012) 4072–4075.
[25] W. Yang, T.P. Fellinger, M. Antonietti, Efficient metal-free oxygen reduction in alkaline medium on high-surface-area mesoporous nitrogen-doped carbons made from ionic liquids and nucleobases, J. Am. Chem. Soc. 133 (2011) 206–209.
[26] H. Masuda, K. Fukuda, Ordered metal nanohole arrays made by a two-step replication of honeycomb structures of anodic alumina, Science 268 (1995) 1466–1468.
[27] J.A. Yopps, D.W. Fuerstenau, The zero point of charge of alpha-alumina, J. Colloid Sci. 19 (1964) 61–71.
[28] J.B. Joo, Y.J. Kim, W. Kim, P. Kim, J. Yi, Simple synthesis of graphitic porous carbon by hydrothermal method for use as a catalyst support in methanol electrooxidation, Catal. Commun. 10 (2008) 267–271.
[29] D. Wei, Y. Liu, Y. Wang, H. Zhang, L. Huang, G. Yu, Synthesis of N-doped graphene by chemical vapor deposition and its electrical properties, Nano Lett. 9 (2009) 1752–1758.
[30] Y. Mao, H. Duan, B. Xu, L. Zhang, Y. Hu, C. Zhao, Z. Wang, L. Chen, Y. Yang, Lithium storage in nitrogen-rich mesoporous carbon materials, Energy Environ. Sci. 5 (2012) 7950–7955.
[31] Y. Lin, Y. Hsu, C. Wu, S. Chen, K.L. Chen, Effects of nitrogen-doping on the microstructure, bonding and electrochemical activity of carbon nanotubes, Diamond Relat. Mater. 18 (2009) 433–437.
[32] C.L. Mangun, J.A. DeBarr, J. Economy, Adsorption of sulfur dioxide on ammonia-treated activated carbon fibers, Carbon 39 (2001) 1689–1696.
[33] V. Gaur, R. Asthana, N. Verma, Removal of SO_2 by activated carbon fibers in the presence of O_2 and H_2O, Carbon 44 (2006) 46–60.
[34] E. Raymundo-Pinero, D. Cazorla-Amoros, A. Linares-Solano, The role of different nitrogen functional groups on the removal of SO_2 from flue gases by N-doped activated carbon powders and fibres, Carbon 41 (2003) 1925–1932.
[35] M. Sevilla, A.B. Fuertes, Sustainable porous carbons with a superior performance for CO_2 capture, Energy Environ. Sci. 4 (2011) 1765–1771.
[36] Z. Wu, P.A. Webley, D. Zhao, Post-enrichment of nitrogen in soft-templated ordered mesoporous carbon materials for highly efficient phenol removal and CO_2 capture, J. Mater. Chem. 22 (2012) 11379–11389.
[37] L.Y. Meng, S.J. Park, Effect of heat treatment on CO_2 adsorption of KOH-activated graphite nanofibers, J.Colloid Interface Sci. 352 (2010) 498–503.
[38] Y.F. Zhao, X. Liu, K.X. Yao, L. Zhao, Y. Han, Superior capture of CO_2 achieved by introducing extra-framework cations into N-doped microporous carbon, Chem. Mater. 24 (2012) 4725–4734.
[39] Q. Li, J.P. Yang, D. Feng, Z.X. Wu, Q.L. Wu, S.S. Park, C.S. Ha, D.Y. Zhao, Facile synthesis of porous carbon nitride spheres with hierarchical three-dimensional mesostructures for CO_2 capture, Nano Res. 3 (2010) 632–642.